Available online at www.sciencedirect.com
ScienceDirect
Journal of Solid State Chemistry 180 (2007) 2845–2850
JOURNAL OF SOLID STATE CHEMISTRY
www.elsevier.com/locate/jssc

Composition dependence of the photophysical and photocatalytic properties of $(AgNbO_3)_{1-x}(NaNbO_3)_x$ solid solutions

Guoqiang Li[a,b,c], Tetsuya Kako[a], Defa Wang[a], Zhigang Zou[b,c], Jinhua Ye[a,*]

[a]*Photocatalytic Materials Center (PCMC), National Institute for Materials Science (NIMS), 1-2-1 Sengen, Tsukuba, Ibaraki 305-0047, Japan*
[b]*Department of Materials Science and Engineering, Nanjing University, Nanjing 210093, PR China*
[c]*Ecomaterials and Renewable Energy Research Center (ERERC), Department of Physics, Nanjing University, Nanjing 210093, PR China*

Received 20 April 2007; received in revised form 30 July 2007; accepted 10 August 2007
Available online 24 August 2007

Abstract

A series of orthorhombic photocatalysts $(AgNbO_3)_{1-x}(NaNbO_3)_x$ solid solutions have been synthesized by a solid-state reaction method. The composition dependence of the photophysical and photocatalytic properties of synthesized solid solutions has been investigated systematically. With an increase in the content of $NaNbO_3$, we found that (1) the lattice parameters decreased; (2) the Nb–O bond length in NbO_6 octahedron reduced; (3) the band gap increased; and (4) the mean particle size decreased while the Brunauer–Emmett–Teller (BET) surface area increased. Photocatalytic activities of the $(AgNbO_3)_{1-x}(NaNbO_3)_x$ ($0 \leqslant x \leqslant 0.5$) samples were evaluated from gaseous 2-propanol (IPA) decomposition into acetone and CO_2 under visible-light irradiation emitted from blue-light-emitting diodes (BLEDs; light intensity: 0.01 mW cm^{-2}). Among all the samples, the $(AgNbO_3)_{0.6}(NaNbO_3)_{0.4}$ sample showed the highest photocatalytic activity.

Keywords: $AgNbO_3$; $NaNbO_3$; Solid solution; Visible-light-sensitive photocatalyst

1. Introduction

Development of visible-light-sensitive photocatalysts has been attracting many attentions in order to utilize solar energy and indoor artificial illuminations effectively [1–6]. Some visible-light-sensitive photocatalysts such as nitrogen-doped TiO_2 and new materials [7–12] have been developed for decomposition of organic compounds. However, a visible-light-sensitive photocatalyst with high activity is still desirable.

For an applicable visible-light-sensitive photocatalyst, high stability under light irradiation and good absorption property to visible light are indispensable. To be a stable photocatalyst, the bottom of its conduction band (CB) energy level should be more negative than the potential of $O_2/O_2^{\bullet -}$. According to the literatures [13,14], the Nb-containing oxides suffice this requirement, so we focus on the Nb-containing oxides. On the other hand, the absorption property to visible light depends on how narrow the band gap is. It is known that Ag 4*d* can hybridize with O 2*p* orbitals, resulting in the lifting up of the top of valence band (VB) [13,15–18]. Therefore, Ag-containing oxides are thought to be good candidates for visible-light-sensitive photocatalysts. Taking into consideration the above two aspects, $AgNbO_3$, where both Nb and Ag are involved, can be considered as one of the plausible candidates. Kato et al. have reported that $AgNbO_3$ has the oxidizing potential to evolve oxygen from an aqueous silver nitrate solution under visible-light irradiation [13]. However, its photocatalytic activity for decomposition of organic compounds is not high. Probably, the valence band potential is not suitable for photodegradation of organics.

In this work, we aimed at improving the photocatalytic activity of $AgNbO_3$ by modifying its crystal structure. It is known that by forming solid solution, crystal and electronic structures of a compound can be successively tuned. We expect that through forming solid solution with

*Corresponding author. Fax: +81 29 859 2301.
E-mail address: Jinhua.YE@nims.go.jp (J. Ye).

0022-4596/$ - see front matter © 2007 Elsevier Inc. All rights reserved.
doi:10.1016/j.jssc.2007.08.006

a proper oxide, the band potential of $AgNbO_3$ can be optimized and its photocatalytic activity can be significantly improved.

To form a solid solution, one should consider the similarity of two end members in the crystal structure, the ionic radius, electronegativity and valence state. Here, $NaNbO_3$ is chosen as the other end member because of the following reasons: the crystal structure of $NaNbO_3$ is similar with that of $AgNbO_3$ which is the perovskite structure with orthorhombic symmetry; the ionic radius of Na is 9.8% smaller than that of Ag, which is smaller than the experiential limitation of 15%; the valence state of Na is +1, the same as that of Ag.

In the present paper, we will report a systematic study on the synthesis and characterization of a series of solid solutions $(AgNbO_3)_{1-x}(NaNbO_3)_x$ $(0 \leqslant x \leqslant 1)$. The composition dependence of the crystal structure, optical absorption property and photocatalytic activities of the solid solutions for organic degradation under visible-light irradiation will be discussed.

2. Experimental section

2.1. Sample preparation

Powder samples of $(AgNbO_3)_{1-x}(NaNbO_3)_x$ $(0 \leqslant x \leqslant 1)$ were synthesized by a conventional solid-state reaction method using Ag_2O (Wako Co., Japan), Na_2CO_3 (Junsei Co., Japan) and Nb_2O_5 (Wako Co., Japan) as starting materials. The well-mixed powders in a stoichiometric ratio with ethanol as medium were dried and preheated at 800 °C for 4 h. Regrinding and subsequent calcinations of the powders at 900 °C for 5 h were repeated for two times. Then we obtained the samples, of which the colors changed from yellow to white with an increase in the content of $NaNbO_3$.

2.2. Characterization

The crystal structures of the synthesized samples were determined by an X-ray diffractometer (JDX-3500; JEOL, Japan) with Cu$K\alpha$ radiation ($\lambda = 1.54178$ Å). Raman scattering spectrum was measured using a laser Raman spectrophotometer (NRS-1000; Jasco, Japan) at room temperature. The power of the incident laser beam was 100 mW with monochromatic wavelength 532 nm. The diffuse reflectance spectrum was recorded with a UV–vis spectrophotometer (UV-2500; Shimadzu Co., Japan) at room temperature and transformed to the absorption spectra according to the Kubelka–Munk relationship. The Kubelka–Munk relationship was expressed as follows: $K/S = (1-R)^2/2R$, where R, K and S are reflectance measurements (relative value to the reference of $BaSO_4$), the absorption and scattering coefficients of sample, respectively [19]. The morphology was observed by using a scanning electron microscope (SEM; JSM-6500; JEOL, Japan). The surface area was analyzed using the Gemini-2360 analyzer (Micromeritics Co., USA) by nitrogen adsorption at 77 K using the Brunauer–Emmett–Teller (BET) method.

2.3. Evaluation of photocatalytic activity

Evaluation of the photocatalytic activity for gaseous 2-propanol (IPA) decomposition was carried out in the 500 ml glass reactor under visible-light irradiation emitted from 12 blue-light-emitting diodes (BLEDs). The spectrum of BLEDs was seen later in the inset of Fig. 7. The light mainly concentrated on the visible-light region at the range of wavelength from 400 to 550 nm. The light intensity was 0.01 mW cm^{-2}, which was determined by a spectroradiometer (USR-40D; Ushio Co., Japan). To remove the organic compounds adsorbed on the surface of the photocatalyst, the samples were pretreated at 150 °C for 30 min in an oven and then cooled to room temperature before use. A 0.4 g of the powders sample was evenly spread over a vessel with 8.1 cm^2 in area, and the vessel was placed on the base of the reactor. After the reactor was sealed and the inside atmosphere was replaced by synthetic air, gaseous IPA with concentration of ca. 370 ppm was introduced into the reactor. The reactor was stored in the dark till the concentration of IPA became unchanged, i.e., the system reached the equilibrium state of adsorption. Finally, the reactor was irradiated with visible light, which was emitted by BLEDs. The concentrations of IPA, acetone and CO_2 were measured using a gas chromatograph (GC-14B; Shimadzu Co., Japan) equipped with a flame ionized detector (FID) and a methanizer. The adsorption property was evaluated from the change of IPA concentration between the initial state and the equilibrium state.

3. Results and discussion

3.1. Crystal structure

Fig. 1 shows the XRD patterns of the $(AgNbO_3)_{1-x}(NaNbO_3)_x$ powder samples at room temperature. The prepared samples were well crystallized into the pseudo-perovskite structure with orthorhombic symmetry. The structure of $AgNbO_3$ consists of a framework of NbO_6 octahedra, the sites between the octahedra being filled with Ag atoms. With the rise in the content of $NaNbO_3$, the positions of diffraction peaks were successively shifted towards larger 2θ, as shown in Fig. 1b. This means that the lattice parameters decreased with increasing amount of $NaNbO_3$, according to the Bragg's Law. From the XRD patterns, the lattice parameters were calculated by the least-squares method applying the structure of $AgNbO_3$. Fig. 2 shows the variations in the lattice parameters and volume of unit cell of synthesized samples. It is clearly seen that the lattice parameters along a, b and c axes and the volumes of unit cell gradually decrease with the increase in the content of $NaNbO_3$. The difference in ionic radius

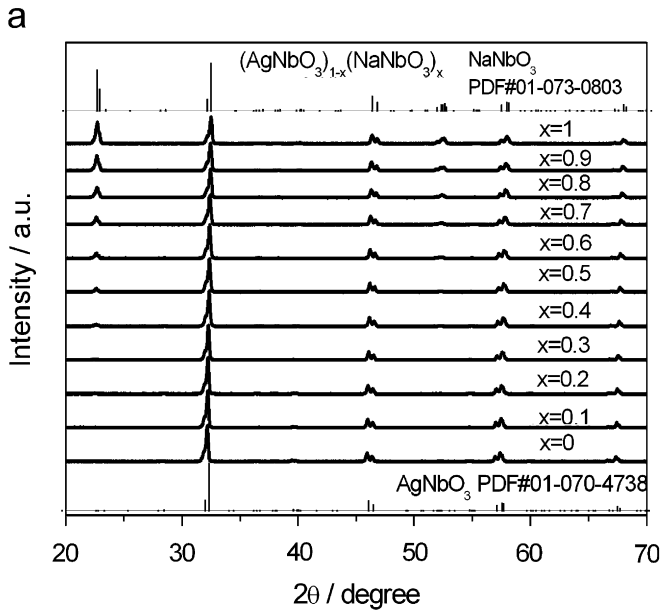

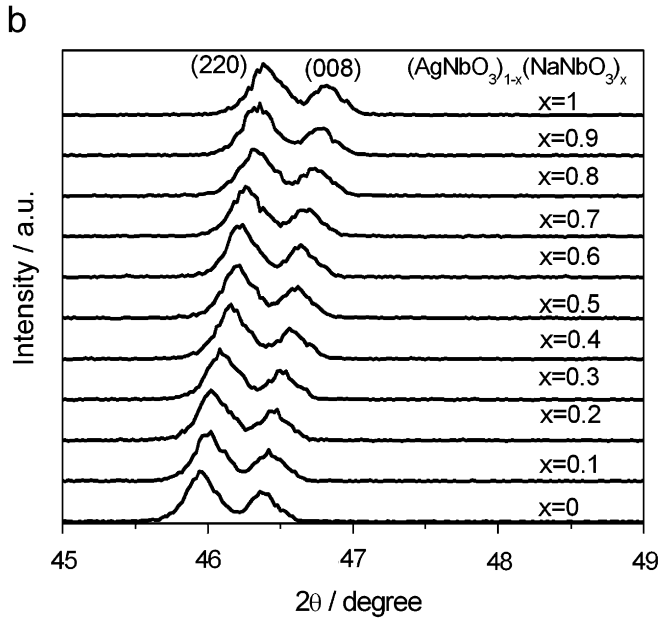

Fig. 1. XRD patterns of $(AgNbO_3)_{1-x}(NaNbO_3)_x$ powder samples (a), and the enlarged view between 45° and 49° (b). As references, the standard XRD patterns for $AgNbO_3$ and $NaNbO_3$ were plotted in Fig. 1a.

between Na and Ag can give a reasonable explanation for all the variations. Since the ionic radius of Na (1.18 Å) is smaller than that of Ag (1.28 Å), the lattice parameters decreased after the Na substitution for Ag in $AgNbO_3$, being consistent with the earlier report [20]. In addition, the intensities of 110 and 118 peaks at 22° and 53° increased with the rise in the amount of $NaNbO_3$. The increase in intensity was caused by the increase of Na occupation in the *A*-site of solid solutions, whose atomic scattering factor differs significantly from that of Ag ion. These results indicated that the $(AgNbO_3)_{1-x}(NaNbO_3)_x$ solid solutions could be formed throughout the whole Na concentration ranges ($0 \leqslant x \leqslant 1$).

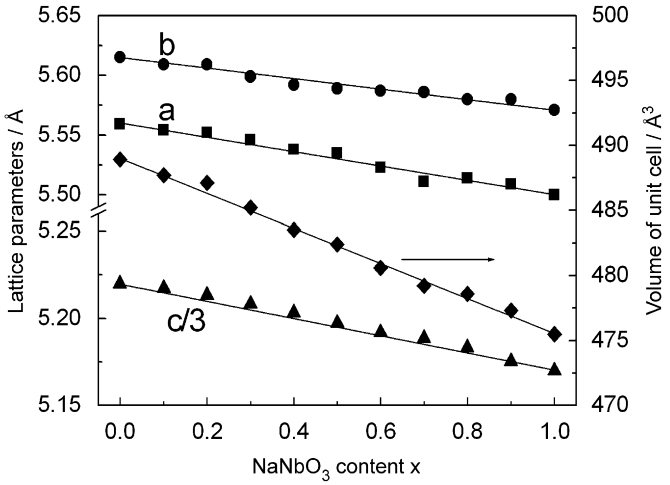

Fig. 2. Variations in lattice parameters (*a*, *b* and *c*) and volume of unit cell of $(AgNbO_3)_{1-x}(NaNbO_3)_x$ solid solutions.

3.2. Raman scattering spectra

Raman scattering is an effective method of investigating the local distortions in the crystal lattice [21]. Fig. 3 shows Raman spectra of the $(AgNbO_3)_{1-x}(NaNbO_3)_x$ solid solutions at a range from 160 to 1000 cm^{-1}. The spectra profiles and the position of the bands for end members of $AgNbO_3$ and $NaNbO_3$ are well agreed with those reported previously [21,22]. The internal vibrations of NbO_6 octahedron generated all bands above 160 up to 900 cm^{-1}. A splitting of the scattered intensities in the region from 170 to 300 cm^{-1} corresponding to degenerated v_6 and v_5 modes was observed. The low intense Raman bands v_4 at ~430 and ~375 cm^{-1} correspond to the associated bending modes of the Nb–O–Nb linkage [23]. The low intensities of these bands indicated that the tilted angle between the adjacent NbO_6 octahedra was low. The second intense Raman band appeared in the 570–605 cm^{-1} region and there was a shoulder in the 520–570 cm^{-1} region. These bands (v_1 and v_2) are assigned to the symmetric stretching modes of NbO_6 octahedron, corresponding to different Nb–O bond lengths [23]. These Raman bands were obviously shifted towards higher wavenumber with the rise in $NaNbO_3$ content. Recently, Shiratori et al. [21] reported that these Raman bands of $NaNbO_3$ shifted towards higher wavenumber with an increase in particle size. In $(AgNbO_3)_{1-x}(NaNbO_3)_x$ solid solutions, however, with an increase in the amount of $NaNbO_3$, these bands shifted to higher wavenumber and the particle sizes tended to decrease, as described in Section 3.4. The shift, consequently, was caused not by the change in particle size, but by the different structure. In other words, the smaller metallic ion Na substitution for the larger ion Ag in $AgNbO_3$ causes the decrease in the Nb–O bond length. It means that the addition of $NaNbO_3$ brings the size of NbO_6 octahedron reducing.

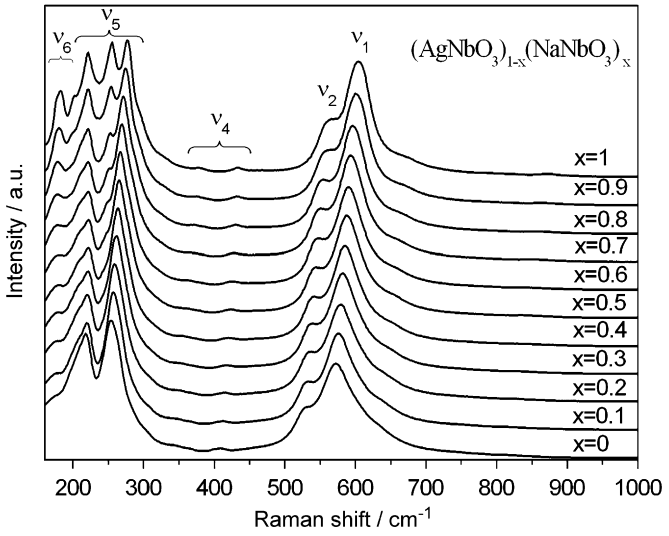

Fig. 3. Raman spectra of $(AgNbO_3)_{1-x}(NaNbO_3)_x$ solid solutions at room temperature.

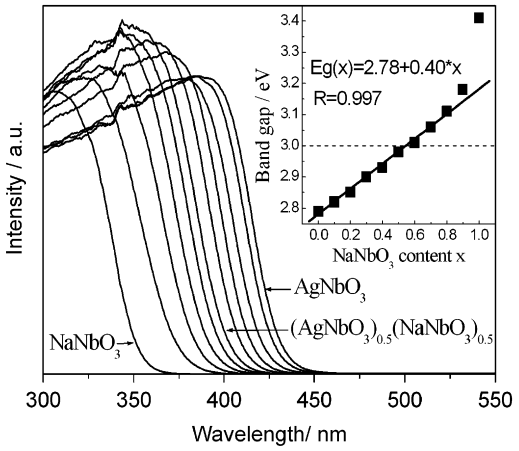

Fig. 4. UV–vis absorption spectra of $(AgNbO_3)_{1-x}(NaNbO_3)_x$ solid solutions. The inset is band gap of $(AgNbO_3)_{1-x}(NaNbO_3)_x$ solid solutions as a function of $NaNbO_3$ content. R is the correlation coefficient.

3.3. Optical property and band gap

As mentioned previously, the band structures of $(AgNbO_3)_{1-x}(NaNbO_3)_x$ solid solutions are expected to be tuned by adjusting the compositions of the samples. Fig. 4 shows the UV–vis optical absorption spectra of the $(AgNbO_3)_{1-x}(NaNbO_3)_x$ solid solutions. With the rise in the content of $NaNbO_3$, the absorption edges were gradually blue-shifted. The optical band gaps could be estimated from the absorption spectra using the following equation [24]:

$$\alpha hv = A(hv - E_g)^{n/2}, \quad (1)$$

where A, α, hv and E_g are constant, absorption coefficient, the photon energy and the optical band gap, respectively. In this equation, n is determined by the transition types and in the case of direct and indirect transition, n is equal to 1 and 4, respectively. The values of n and E_g were estimated by the following steps [16]: first, the plot of $\ln(\alpha hv)$ vs. $\ln(hv-E_g)$ was drawn using an approximate value of E_g, and then the value of n was estimated from the slope of the straight line near the band edge; second, the plot of $(ahv)^{2/n}$ vs. hv was drawn and then a tangential line was plotted near the band edge, the x-intercept of the tangential line corresponded to the optical band gap. By using this method, the value of n was estimated to equal 4. The inset of Fig. 4 shows the variation in the optical band gaps estimated. The correlation coefficient, R that suggested the degree of a linear relationship between the two variables (E_g and x ($x<0.8$)) was 0.997 (see the inset of Fig. 4). Because this value was close to 1, it was clearly seen that the band gaps increased almost linearly with the rise in the content of $NaNbO_3$. The regression equation was able to be written as follows:

$$E_g(x) = 2.78 + 0.40x. \quad (2)$$

From this equation, we know that the $(AgNbO_3)_{1-x}(NaNbO_3)_x$ ($0 \leqslant x \leqslant 0.5$) samples are visible-light-sensitive materials ($E_g \leqslant 3.0$ eV).

The band gap was increased with an increasing amount of $NaNbO_3$, because the contribution of Ag 4d orbital to the top of valence band became smaller. The conduction band energy levels of $AgNbO_3$ and $NaNbO_3$ were reported to locate at -0.4 eV (vs. NHE) [13]. Taking into account the band gap energies of $AgNbO_3$ (2.79 eV) and $NaNbO_3$ (3.4 eV), the top of valence band energy levels of solid solutions $(AgNbO_3)_{1-x}(NaNbO_3)_x$ ($0 \leqslant x \leqslant 1$) would locate between $+2.39$ and $+3.00$ eV. It means that the top of valence band energy level in solid solutions are more positive than that of $AgNbO_3$. In general, the top of valence band energy level determines the oxidizing power; and the more positive the top of valence band energy level, the stronger the oxidizing power. Therefore, it is apparent that the oxidizing power of $(AgNbO_3)_{1-x}(NaNbO_3)_x$ ($0 \leqslant x \leqslant 0.5$) is stronger in comparison with that of $AgNbO_3$. Due to the stronger oxidizing power, the solid solutions are expected to show the improved photocatalytic activities for decomposition of organic compounds compared with that of $AgNbO_3$.

3.4. Morphology and surface area

Fig. 5 shows the SEM images of $AgNbO_3$, $(AgNbO_3)_{0.6}(NaNbO_3)_{0.4}$ and $NaNbO_3$. The mean particle sizes of $AgNbO_3$, $(AgNbO_3)_{0.6}(NaNbO_3)_{0.4}$ and $NaNbO_3$ were estimated to be 1.5, 1.0 and 0.6 μm, respectively. Consistently, BET surface areas tended to increase with the rise in the amount of $NaNbO_3$, as shown in Fig. 6. Assuming that the samples consisted of the sphere particles, the BET equivalent particle sizes of $AgNbO_3$ and $NaNbO_3$ could be estimated to be 1.4 and 0.7 μm, respectively [25,26]. This is well agreed with the SEM results. Clearly, the addition of $NaNbO_3$ was favorable for the reduction in the particle sizes of solid solutions.

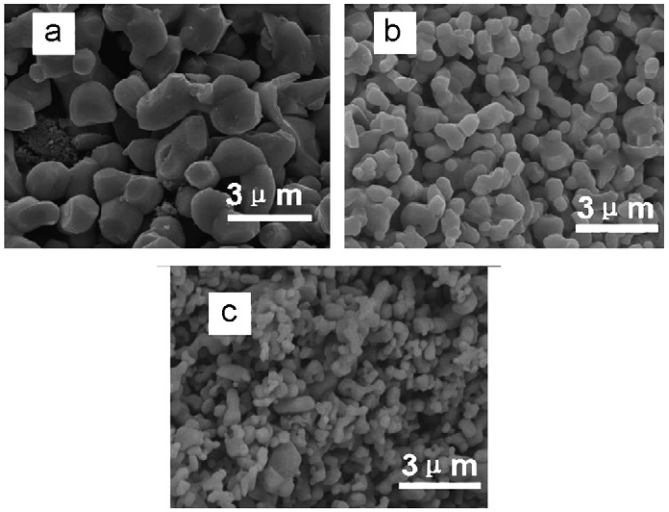

Fig. 5. SEM images of $AgNbO_3$ (a), $(AgNbO_3)_{0.6}(NaNbO_3)_{0.4}$ (b) and $NaNbO_3$ (c).

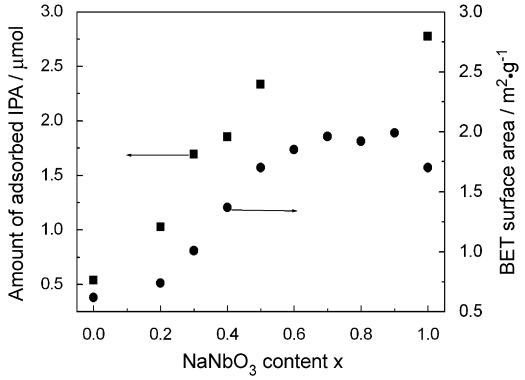

Fig. 6. Amount of adsorbed IPA and BET surface area as a function of $NaNbO_3$ content in $(AgNbO_3)_{1-x}(NaNbO_3)_x$.

3.5. Adsorption property

The different surface areas of $(AgNbO_3)_{1-x}(NaNbO_3)_x$ solid solutions were expected to have different adsorption properties. Fig. 6 shows the amount of adsorbed IPA as a function of the $NaNbO_3$ content. When the content of $NaNbO_3$ increased from 0 to 0.5, the amount of adsorbed IPA increased from 0.5 to 2.5 μmol. Apparently, the improvement in the adsorption properties should be ascribed to the increase in the surface area.

3.6. Photocatalytic property

Photocatalytic activity was evaluated from the decomposition of gaseous IPA into acetone under visible-light irradiation emitted from BLEDs, the spectrum of which is shown in the inset of Fig. 7. As shown in Fig. 7, the acetone evolution rate increased from 0.8 to 2.8 ppm h^{-1} when the content of $NaNbO_3$ rose from 0 to 0.4, whereas the acetone evolution rate decreased when the content of $NaNbO_3$ further increased from 0.4 to 1. It is worthy to note that all

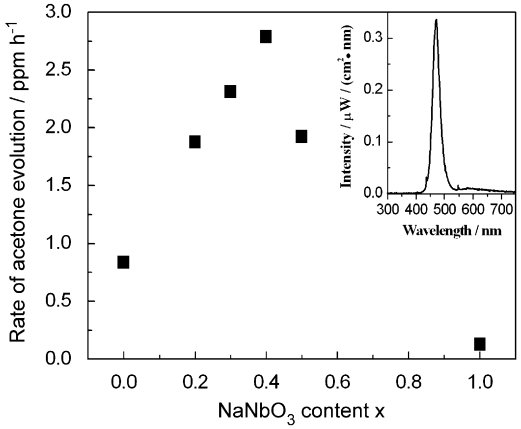

Fig. 7. Rate of acetone evolution under visible-light irradiation as a function of $NaNbO_3$ content in $(AgNbO_3)_{1-x}(NaNbO_3)_x$. The inset is the spectrum of BLEDs. The light intensity is 0.01 mW cm^{-2}.

the solid solutions $(AgNbO_3)_{1-x}(NaNbO_3)_x$ ($x = 0.2$, 0.3, 0.4 and 0.5) with the visible-light absorption show significantly enhanced activities in comparison with the end members, $AgNbO_3$ and $NaNbO_3$. Among all samples tested, the $(AgNbO_3)_{0.6}(NaNbO_3)_{0.4}$ sample showed the highest visible-light photocatalytic activity for gaseous IPA decomposition, and the activity of this sample was three times over that of $AgNbO_3$.

The photocatalytic activity of $(AgNbO_3)_{1-x}(NaNbO_3)_x$ solid solutions for decomposition of organic compounds under visible-light irradiation was influenced by the oxidizing power determined by the top of valence band, particle size (surface area) and visible-light absorption capability. When the content of $NaNbO_3$ in $(AgNbO_3)_{1-x}(NaNbO_3)_x$ solid solutions increased, the oxidizing power increased and the particle size reduced, both of them would lead to an enhancement of photocatalytic activity. On the other hand, the visible-light absorption capability became weaker, which would result in a decrease in photocatalytic activity. In the sample $(AgNbO_3)_{0.6}(NaNbO_3)_{0.4}$, the competition among the oxidizing power, particle size and visible-light absorption is considered to have achieved an optimum state, resulting in the highest visible-light photocatalytic activity of this material.

To further check the oxidization property of solid solutions, we investigated the process of IPA mineralization over $(AgNbO_3)_{0.7}(NaNbO_3)_{0.3}$ sample. Fig. 8 shows the changes in gases concentrations as a function of irradiation time under visible-light irradiation. The concentrations of acetone and CO_2 increased with the irradiation time while that of IPA decreased, indicating that IPA could be mineralized to CO_2 by the $(AgNbO_3)_{0.7}(NaNbO_3)_{0.3}$ photocatalysis. The rates of acetone and CO_2 evolution on $(AgNbO_3)_{0.7}(NaNbO_3)_{0.3}$ were estimated to be ~2.3 and ~0.3 ppm h^{-1}, respectively. It is apparent that the rate of acetone evolution is higher than that of CO_2, indicating that the photocatalytic decomposition of IPA to acetone is easier than that of acetone to CO_2, because the photocatalytic decomposition of IPA to acetone is one hole

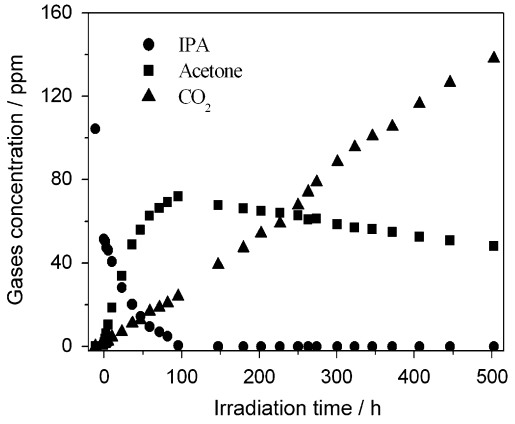

Fig. 8. Variations in gases concentration over $(AgNbO_3)_{0.7}(NaNbO_3)_{0.3}$ under visible-light irradiation emitted from BLEDs. The light intensity is 0.01 mW cm^{-2}. The initial concentration of IPA is 105 ppm.

reaction while the reaction of acetone to CO_2 is a more complex multi-hole involved process [27–29].

4. Conclusions

We investigated the composition dependence of crystal structure, photophysical and photocatalytic properties of $(AgNbO_3)_{1-x}(NaNbO_3)_x$ solid solutions. With an increase in the content of $NaNbO_3$, the lattice parameters and Nb–O bond length in NbO_6 octahedron are reduced. The hybridization ratio of Ag 4*d* and O 2*p* decreases and thus the valence band top moves to the more positive direction, leading to a blue shift in the optical absorption edge and an enhancement of oxidizing power. The addition of $NaNbO_3$ also causes a decrease in particle size and hence an increase in BET surface area. The highest visible-light photocatalytic activity for decomposition of IPA into acetone was obtained over $(AgNbO_3)_{0.6}(NaNbO_3)_{0.4}$ sample, in which the competition among the oxidizing power, particle size and visible-light absorption was considered to have achieved an optimum state.

Acknowledgments

The present research was partially supported by the Global Environment Research Fund of the Japanese Government. And it was also supported by the National Natural Science Foundation of China (No. 20528302) and the Jiangsu Provincial Natural Science Foundation (Nos. BK2006718 and BK2006127). Prof. Z.G. Zou would like to thank the Jiangsu Provincial Talent Scholars Program.

References

[1] M.R. Hoffmann, S.T. Martin, W. Choi, D.W. Bahnemann, Chem. Rev. 95 (1995) 69–96.
[2] A.L. Linsebigler, G.Q. Lu, J.T. Yates, Chem. Rev. 95 (1995) 735–758.
[3] J.M. Herrmann, Top. Catal. 34 (2005) 49–65.
[4] R. Asahi, T. Morikawa, T. Ohwaki, K. Aoki, Y. Taga, Science 293 (2001) 269–271.
[5] Z. Zou, J. Ye, K. Sayama, H. Arakawa, Nature 414 (2001) 625–627.
[6] K. Maeda, K. Teramura, D. Lu, T. Takata, N. Saito, Y. Inoue, K. Domen, Nature 440 (2006) 295.
[7] H. Irie, Y. Watanabe, K. Hashimoto, J. Phys. Chem. B 107 (2003) 5483–5486.
[8] J. Tang, Z. Zou, J. Ye, Angew. Chem. Int. Ed. 43 (2004) 4463–4466.
[9] H. Kim, D. Hwang, J. Lee, J. Am. Chem. Soc. 126 (2004) 8912–8913.
[10] M. Miyauchi, M. Takashio, H. Tobimatsu, Langmuir 20 (2004) 232–236.
[11] T. Kako, J. Ye, Mater. Trans. 46 (12) (2005) 2694–2698.
[12] Y. Maruyama, H. Irie, K. Hashimoto, J. Phys. Chem. B 110 (2006) 23274–23278.
[13] H. Kato, H. Kobayashi, A. Kudo, J. Phys. Chem. B 106 (2002) 12441–12447.
[14] D.E. Scaife, Sol. Energy 25 (1980) 41–54.
[15] A.A. Ivantsov, A.V. Soldatov, Yu.V. Sukhetskii, A.N. Gusatinskii, A.P. Kovtun, Phys. Status Solidi 164 (1991) K23–K25.
[16] J. Tang, Z. Zou, J. Ye, J. Phys. Chem. B 107 (2003) 14265–14269.
[17] T. Murase, H. Irie, K. Hashimoto, J. Phys. Chem. B 109 (2005) 13420–13423.
[18] S. Ouyang, H. Zhang, D. Li, T. Yu, J. Ye, Z. Zou, J. Phys. Chem. B 110 (2006) 11677–11682.
[19] P. Kubelka, F. Munk, Z. Technol. Phys. 12 (1931) 593–601.
[20] A. Kania, J. Kwapuliński, J. Phys.: Condens. Matter 11 (1999) 8933–8946.
[21] Y. Shiratori, A. Magrez, J. Dornseiffer, F. Haegel, C. Pithan, R. Waser, J. Phys. Chem. B 109 (2005) 20122–20130.
[22] A. Kania, K. Roleder, G.E. Kugel, M.D. Fontana, J. Phys. C: Solid State Phys. 19 (1986) 9–20.
[23] J. Jehng, I. Wachs, Chem. Mater. 3 (1991) 100–107.
[24] M. Butler, J. Appl. Phys. 48 (1977) 1914–1920.
[25] Using the relationship $d = 6/(\mathrm{BET} \times \rho)$ [20], where d and ρ is the BET equivalent particle size and the theoretical density. The theoretical densities of $NaNbO_3$ and $AgNbO_3$ were 4.57 [20] and 6.80 g cm^{-3} [26], respectively.
[26] J. Fabry, Z. Zikmund, A. Kania, V. Petricek, Acta Crystallogr. C 56 (2000) 916–918.
[27] J.M. Coronado, S. Kataoka, I. Tejedor-Tejedor, M.A. Anderson, J. Catal. 219 (2003) 219–230.
[28] F. Arsac, D. Bianchi, J.M. Chovelon, C. Ferronato, J.M. Herrmann, J. Phys. Chem. A 110 (12) (2006) 4202–4212.
[29] F. Arsac, D. Bianchi, J.M. Ch.ovelon, C. Ferronato, J.M. Herrmann, J. Phys. Chem. A 110 (12) (2006) 4213–4222.